

A Switched-Gain Nonlinear Observer for LED Optical Communication ^{*}

Ibrahima N'Doye^{*} Ding Zhang^{*,**} Ali Zemouche^{***}
Rajesh Rajamani^{****} Taous-Meriem Laleg-Kirati^{*}

^{*} *Computer, Electrical and Mathematical Sciences and Engineering
Division (CEMSE), King Abdullah University of Science and
Technology (KAUST), Thuwal 23955-6900, Saudi Arabia, (e-mail:
ibrahima.ndoye@kaust.edu.sa; taousmeriem.laleg@kaust.edu.sa).*

^{**} *Department of Electronic and Computer Engineering, The Hong
Kong University of Science and Technology, Clear Water Bay,
Kowloon, Hong Kong, China, (e-mail: ding.zhang@connect.ust.hk)*

^{***} *University of Lorraine, CRAN CNRS UMR 7039, 54400 Cosnes et
Romain, France, (e-mail: ali.zemouche@univ-lorraine.fr)*

^{****} *Department of Mechanical Engineering, University of Minnesota,
MN 55455 USA, (e-mail: rajamani@me.umn.edu)*

Abstract: Alignment for maintaining Line-of-Sight (LoS) between the receiver and the transmitter in a LED optical communication system is a challenging problem due to the constant movement of the underlying optical platform that is caused by vibration effects and atmospheric turbulence. In this paper, we propose a robust switched-gain nonlinear observer to estimate the angular position and velocity of the receiver orientation, which is used subsequently to follow the receiver orientation. The optical communication system model involves highly nonlinear and non-monotonic output measurement equations. Furthermore, tracking the receiver with perfect alignment results in loss of local observability. Hence, a two-receiver system is utilized to provide a robust tracking system that retains observability over the entire range of operation of the system. Lyapunov function-based analysis that ensures global stability is used to design the observer; then, a static feedback controller drives the receiver orientation based on the state estimate. Finally, numerical simulations are presented on the performance of the observer-based static feedback control in accurately estimating and tracking the angular position and velocity of the receiver orientation.

Keywords: Light-emitting diode (LED)-based optical communication model, nonlinear systems, nonlinear observer design, monotonic systems, hybrid systems, linear matrix inequality (LMI).

1. INTRODUCTION

Over the last decade, many research efforts have been devoted towards advancing Optical Wireless Communication (OWC) technology. OWC is considered as a promising paradigm in the communication area. In fact, compared to radio-frequency and acoustic communication systems, OWC is able to provide: low latency, low cost and power consumption, high data rates (Hanson and Radic (2008); Hagem et al. (2011); Lu et al. (2009)).

Most communication for above-ground robots and devices occurs through RF communication. However, in the case of underwater robots, RF (radio waves) cannot propagate long distances underwater. Other means of wireless communication are needed. The most common method for underwater wireless communication is through acoustic waves. However, acoustic multi-path phenomena is a problem with acoustic waves. In addition, large latency and

low bandwidth are other disadvantages. Hence, LED-based visual light communication is an alternate choice that is being recently pursued for underwater communication. Further, optical wireless communication is also now starting to be pursued as an alternative and/or complementary technology for above-ground RF wireless solutions, especially for the "last mile" and "last-leg" problems in networks. In particular, line-of-sight links have the highest data rates and are therefore an attractive communication option.

Previous results on the Extended Kalman Filter (EKF)-based algorithm of maintaining active alignment control for light-emitting diode (LED)-based wireless optical communications lack theoretical guarantees of the convergence of the estimator (Solanki et al. (2016, 2018)). Indeed, small errors in the output measurement can make the EKF system go unstable. Hence, we propose a robust nonlinear observer to estimate the angle and the velocity of the receiver orientation in this paper. The proposed nonlinear hybrid observer-based static feedback control is computationally efficient and guarantees sufficient stability conditions.

^{*} This work has been supported by the King Abdullah University of Science and Technology (KAUST), Base Research Fund (BAS/1/1627-01-01) to Taous Meriem Laleg.

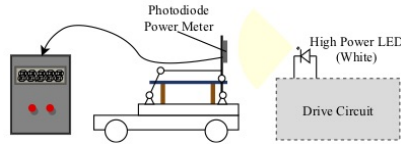


Fig. 1. Schematic diagram of the LED-based communication.

In this paper, we envision a scenario in which a group of mobile vehicle robotic agents is used for mobile networking sensing applications. Our research aims at designing a robust observer-based control for nonlinear systems with nonlinear output equations to estimate and track the angle between the receiver aperture and the LoS beam sent by the transmitter for a LED-based optical communication system. To ensure global asymptotic stability, we derive constant stabilizing observer gain in each piecewise monotonic regions. Furthermore, the proposed observer design can be integrated into small ground mobile vehicle robots for mobile networking sensing applications.

The outline of the rest of the paper is as follows. In section 2, the optical channel modeling of the LED system is presented, which includes the description of the experimental system setup, the luminous flux model and its model calibrated, the state space formulation and analysis. In section 3, the observer design is presented, which ensures the asymptotic convergence of the estimation error. Based on the state estimate, a static feedback controller updates the receiver orientation. Simulation results of the robust observer-based tracking are presented in section 5. Finally, concluding remarks are shown in section 6.

2. LED-BASED OPTICAL CHANNEL MODELING

The LED-based optical channel describes a two-way communication that consists of a single LED transmitter and a single photodiode receiver; each end can rotate by an angle in which it establishes and maintains LoS. In this section, we describe the experimental setup for an estimation problem of LED-based optical channel modeling. We discuss the luminous flux model, and finally, we formulate the state-space representation, which takes the form of a dynamical system with a nonlinear output map.

2.1 System Setup

Studies on the radiation pattern of LED shows that the radiation region of the LED source can be separated into the near field and far field by the LED-to-target distance, in which the patterns have significant differences (Ivan and Ching-Cherng (2008)). A high-power LED can have 20 mm near to midfield, in which region the radiation pattern is distance-dependent while it will not change in far-field. As the range of communication is far longer than 20 mm, here we treat radiation pattern as distance-invariant and try to obtain the spatial distribution of LED luminous flux for our specific system setup as shown in Fig. 1.

2.2 Luminous Flux Model

The spatial distribution model of LED luminous flux has been studied for a long time (Ghassemlooy et al. (2012); Doniec et al. (2013); Solanki et al. (2018)). The

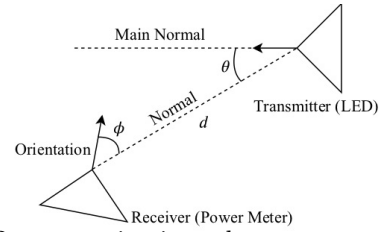


Fig. 2. LED communication scheme

model mainly describes the effect of relative position and orientation between the transmitter and the receiver on the signal strength. Typically, the relative position between transmitter and receiver is expressed with three parameters: the distance d between them, the angle θ between normal direction and the main normal direction of transmitter, and the angle ϕ between the orientation of receiver and the normal direction. Fig. 2 illustrates the variables of interest, which include the transmission distance d , the transmission angle θ , and the angle of incidence of ϕ .

The incident power on the detector can be determined based on the signal irradiance at the relative detector position. The full signal strength model can be formulated as follows (Ghassemlooy et al. (2012); Doniec et al. (2013); Solanki et al. (2016, 2018))

$$P_d = CI(\theta, d) \exp(-cd)g(\phi), \quad (1)$$

where P_d is the measurement of power, which is proportional to the luminous flux of light that is detected by the receiver, C and c are both constants. The $\exp(-cd)$ portion comes from Beer-Lambert's law (Miller et al. (2009)) which describes the attenuation of power when light travels through medium as an exponential decay; $I(\theta, d)$ is usually in the following form (Ghassemlooy et al. (2012); Doniec et al. (2013); Solanki et al. (2016, 2018))

$$I(\theta, d) = I(0, d) \cos^m(\theta)/d^2, \quad (2)$$

where $I(0)$ is the central luminous flux, as well as the maximum luminous flux and m , is the order of Lambertian emission

$$m = \frac{\ln(2)}{\ln \cos(\theta_{1/2})}.$$

In the above formula, $\theta_{1/2}$ is the angle at half the illuminance of an LED. Physically, $I(0, d) \cos^m(\theta)$ represents the radiation pattern of LED source (Ivan and Ching-Cherng (2008)) and the reciprocal of d^2 comes from the inverse-square law which describes the geometric dilution of a physical quantity.

2.3 Model Calibration

To derive the LED model, the first step is to parameterize the LED-based optical model (1). We have conducted experiments to measure the luminous flux of a high-power LED module at different relative positions in a clear and windless air condition when there is a relative motion between the receiver and the transmitter. We designed three groups of experiments to estimate the unknown parameters of the luminous flux model given in (1).

Measured Signal Strength Versus Transmitter-Receiver Distance The LED source is fixed at the center of concentric circles, as shown in Fig. 3, and the main normal

Table 1. Fitting Results

Terms	Model	Parameters						R^2	RMSE
		$a(a_1)$	$b(b_1)$	$c(c_1)$	a_2	b_2	c_2		
Scattering, absorption, dilution	$a \exp(-bx)/x^2$	0.01009	1.972	-	-	-	-	0.9947	0.0058
Receiver orientation	$a_1 \exp\left[-\left(\frac{x-b_1}{c_1}\right)^2\right] + a_2 \exp\left[-\left(\frac{x-b_2}{c_2}\right)^2\right]$	0.9953	0.06298	0.2517	0.2260	-0.1995	0.132	0.9970	0.0205

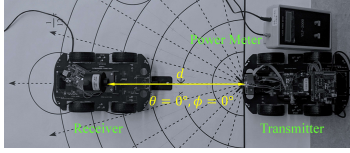


Fig. 3. Transmitter-receiver distance setup in free-space.

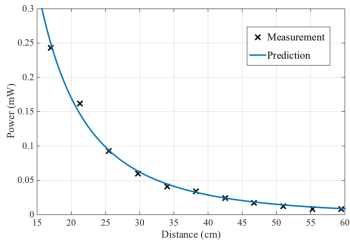


Fig. 4. Measured signal strength versus the transmitter-receiver distance in free-space.

direction of LED is aligned with the symmetric axis. To observe the impact of the distance in the optical communication link, the receiver car is placed at eleven equidistant points, respectively. At each location, we took five samples of measured power and computed their means and variances.

As shown in Fig. 4, the signal strength declines when the distance between the receiver and the transmitter increases. Besides, the nonlinear model $a \exp(-bx)/x^2$, which combines the effects of absorption, scattering, and geometric dilution, fits well with the measured signal strength data.

$$P_d(d, 0, 0) = a \frac{\exp(-bd)}{d^2}, \quad (3)$$

where a and b are the curve fitting parameters defined in Table 1.

Angular Transmission Intensity Distribution Assuming that the maximum power at a distance d_0 is achieved when $\theta = 0^\circ$, we define the power ratio \tilde{I}_θ as follows

$$\tilde{I}_\theta := \frac{I(\theta, d_0)}{I(0, d_0)}. \quad (4)$$

Using the fact that the angular intensity distribution of the transmitter is rotationally symmetric with the LED's normal ($\theta = 0^\circ$), then we can measure the intensity of all the points at the same radial distance based on spatial power ratio intensity distribution \tilde{I}_θ . Hence, at a unit distance, we assume that \tilde{I}_θ is known and represents the light intensity for different transmitter angles.

Measured Signal Strength Versus Incidence Angle ϕ The high power LED source is aligned with the center of the detector point and targeted at the main normal direction. To obtain an approximate form of $g(\phi)$, we place the receiver along a circle to maintain the distance d constant

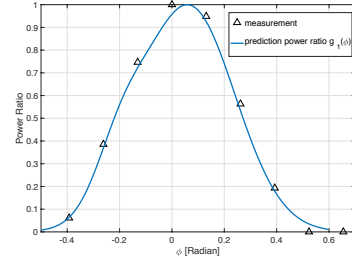


Fig. 5. Gaussian curve fitting the incidence angle ϕ .

and the transmission angle θ constant and known at all times.

In this scenario, θ and the distance d are actually set to 0° and 34 cm, respectively. $g(\phi)$ is a unimodal function which represents empirically the power ratio. Assume that at ϕ_0 , $g(\phi)$ reaches its maximum $g(\phi_0) = 1$, then we can have

$$\frac{P_d(0.34, 0, \phi)}{P_d(0.34, 0, \phi_0)} = \frac{g(\phi)}{g(\phi_0)} = g(\phi). \quad (5)$$

A proper function $g(\phi)$ fitting measured data is composed of two Gaussian terms with six unknowns, as shown in Fig. 5. The curve fitting could be done using a single Gaussian mode, but having one extra Gaussian model gives significantly better fitting. Using MATLAB curve fitting tool which is based on Least Square method, we can evaluate $g(\phi)$ as follows

$$g(\phi) \approx a_1 \exp\left[-\left(\frac{\phi - b_1}{c_1}\right)^2\right] + a_2 \exp\left[-\left(\frac{\phi + b_2}{c_2}\right)^2\right], \quad (6)$$

where a_1 , a_2 , b_1 , b_2 , c_1 and c_2 are the curve fitting parameters defined in Table 1.

Now the resulting luminous flux model is obtained by combining equations (3), (4) and (6) into a compact model.

$$P_d(d, \theta, \phi) = \underbrace{\frac{a \exp(-bd)}{d^2}}_{\text{Transmitter}} \tilde{I}_\theta \underbrace{g_1(\phi)}_{\text{Receiver}}. \quad (7)$$

From (7), we can evaluate the luminous flux generated by LED source at given d and θ with ϕ set to 0° , i.e. the receiver's pointing error is set to zero. Then, we transform from polar frame to cartesian coordinates ($x = d \cos \theta$, $y = d \sin \theta$), and the spacial distribution of LED-based luminous flux in 2-D space.

2.4 State-Space Formulation

From (7), we formulate the state space representation based on the two variables of interest ϕ , and $\dot{\phi}$ that relate to the angles of the receiver. On the other hand, we note that practically it not easy to move the distance d ideally because it needs to move the whole robot. Besides, controlling the angular velocity of $\dot{\phi}$ is more practical. The

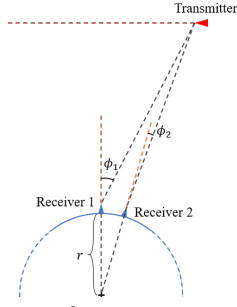


Fig. 6. Measurements of two receivers ϕ_1 and ϕ_2 .

robot alignment is performed by stabilizing the angular velocity.

Since the distance d cannot be adjusted easily and θ fixed, therefore, our states variables are defined as follows

$$x = \begin{bmatrix} x_1 \\ x_2 \end{bmatrix} = \begin{bmatrix} \phi \\ \dot{\phi} \end{bmatrix}. \quad (8)$$

We assume that the dynamic is slow and subject to a gaussian process. The representation in the discrete-time domain can be written as follows

$$x_k = \begin{bmatrix} x_{1,k} \\ x_{2,k} \end{bmatrix} = \begin{bmatrix} x_{1,k-1} + x_{2,k-1} + w_{1,k-1} \\ x_{2,k-1} + u_{k-1} + w_{2,k-1} \end{bmatrix}, \quad (9)$$

where $w_{1,k}$ and $w_{2,k}$ are the process noises which are assumed to be white independent Gaussian noises. u_k is the control input in which modifies the receiver's angular velocity. The measurement $P_{d,k}$ is expressed as

$$y_k = P_{d,k} = \bar{C}_p g(x_{1,k}) + v_k, \quad (10)$$

where $\bar{C}_p = C_p \tilde{I}_\theta \exp(-cd_0)/d_0^2$, g is defined in (6) and v_k is an additive white Gaussian noise.

2.5 Non-Existence of a Constant Observer Gain for Non-Monotonic Systems

The following lemma provides the non-existence of a constant observer gain solution for the non-monotonic LED-based optical communication model.

Lemma 1. (Movahedi et al. (2019); Rajamani et al. (2020)) The discrete-time LED model (9) and (10) is a single output nonlinear system and the output function is non-monotonic as shown in Fig. 5, then a constant gain observer does not exist.

The system seems to be locally unobservable at $\phi = 0^\circ$. Hence, we introduce an additional receiver on the same robot with a constant shifted angle of $\Delta\phi$ to achieve observability, as illustrated in Fig. 6. This shifted angle is added to account for the actual orientation of the receiver. At each movement of the transmitter platform, the states are updated according to the system dynamics. Both ϕ_1 and $\phi_2 = \phi_1 + \Delta\phi$ can be controlled to 0° , when ϕ_1 is controlled to 0° and reads the wirelessly transmitted data, its orientation is being maintained by using ϕ_2 .

The resulting output vector can be written as follows

$$y_k = \bar{C}_p \begin{bmatrix} g(x_{1,k}) \\ g(x_{1,k} + \Delta\phi) \end{bmatrix} + v_k. \quad (11)$$

3. NONLINEAR OBSERVER DESIGN: A GENERAL SYNTHESIS METHOD

First, we derive the theoretical results on the robust observer design procedure for a class of nonlinear monotonic output equations system. Then, we present a robust hybrid observer design methodology that enables stable observers for the non-monotonic output functions of the LED optical communication systems. Finally, a static feedback control gain is evaluated to drive the mean of the receiver orientation to zero based on the state estimate.

3.1 System Description

Motivated by the LED-based optical communication model with nonlinear output equations and measurements Gaussian noises described in (9), we propose the following discrete-time model

$$\begin{cases} x_{k+1} = Ax_k + Bu_k + Ew_k \\ y_k = h(x_k) + Dw_k \end{cases} \quad (12)$$

where $x_k \in \mathbb{R}^n$ is the state vector, $y_k \in \mathbb{R}^p$ is the output measurement, $u_k \in \mathbb{R}^m$ is an input vector, $w_k \in \mathbb{R}^z$ is the disturbance \mathcal{L}_2 bounded vector and the matrices $A_i \in \mathbb{R}^{n \times n}$, $B \in \mathbb{R}^{n \times m}$, $E \in \mathbb{R}^{n \times z}$ and $D \in \mathbb{R}^{p \times z}$ are constant. The nonlinear output function $h : \mathbb{R}^n \rightarrow \mathbb{R}^p$ is assumed to be globally Lipschitz.

The estimation problem aims to get the states that will guide the controller to the normal direction.

3.2 Observer Design

To estimate the unmeasurable state variables of the model (12), we use the following nonlinear observer structure

$$\hat{x}_{k+1} = A\hat{x}_k + Bu_k + L(y_k - h(\hat{x}_k)), \quad (13)$$

where \hat{x}_k is the estimate of x_k . The matrix $L \in \mathbb{R}^{n \times p}$ is the observer gain parameter to be determined later.

Since $h(\cdot)$ is globally Lipschitz, then, there exist $z_i \in Co(\vartheta_i, \hat{\vartheta}_i)$, functions $\phi_{ij} : \mathbb{R}^{n_i} \rightarrow \mathbb{R}$, and constants a_{ij}, b_{ij} , such that (Draa et al. (2019))

$$h(x) - h(\hat{x}) = \sum_{i,j=1}^{p,n_i} \phi_{ij}(z_i) \mathcal{H}_{ij}(\vartheta_i - \hat{\vartheta}_i), \text{ and} \quad (14)$$

$$\hat{\vartheta}_i = H_i \hat{x}_k, a_{ij} \leq \phi_{ij}(z_i) \leq b_{ij}, \phi_{ij}(z_i) = \frac{\partial h_i}{\partial \vartheta_i^j}(z_i), \quad (15)$$

where

$$\mathcal{H}_{ij} = e_p(i) e_{n_i}^T(j), \quad \phi_{ij} \triangleq \phi_{ij}(z_i), \quad (16)$$

$H_i \in \mathbb{R}^{n_i \times n}$, $Co(\vartheta_i, \hat{\vartheta}_i)$ is the convex hull of $(\vartheta_i, \hat{\vartheta}_i)$ and $e_s(i) = (\underbrace{0, \dots, 0}_{s \text{ components}}, 1, 0, \dots, 0)^T \in \mathbb{R}^s, s \geq 1$ is a vector of the canonical basis of \mathbb{R}^s .

Since $\vartheta_i - \hat{\vartheta}_i = H_i e_k$ and for all $i = 1, \dots, p$ and $j = 1, \dots, n_i$, we can rewrite the nonlinearities as follows

$$h(x_k) - h(\hat{x}_k) = \sum_{i,j=1}^{p,n_i} \phi_{ij} \mathcal{H}_{ij} H_i e_k \triangleq C e_k + \sum_{i,j=1}^{p,n_i} \tilde{\phi}_{ij} \mathcal{H}_{ij} H_i e_k,$$

where

$$C \triangleq \sum_{(i,j) \in \mathfrak{F}} a_{ij} \mathcal{H}_{ij} H_i, \quad \tilde{\phi}_{ij} \triangleq \phi_{ij} - a_{ij}, \quad \mathfrak{F} \triangleq \{(i,j) : a_{ij} \neq 0\}.$$

Therefore, the dynamic equation of the estimation error can be written as

$$\begin{aligned} e_{k+1} &= \underbrace{\left(A + L \sum_{i,j=1}^{p,n_i} [\tilde{\phi}_{ij} \mathcal{H}_{ij} H_i] \right)}_{\mathbb{A}} e_k + \underbrace{(E - LD)}_{\mathbb{E}} w_k \\ &= (A - LC) e_k + \mathbb{E} w_k - \sum_{i,j=1}^{p,n_i} \tilde{\phi}_{ij} L \mathcal{H}_{ij} H_i e_k. \end{aligned} \quad (17)$$

It follows that

$$0 \leq \tilde{\phi}_{ij} \leq \tilde{b}_{ij} \triangleq b_{ij} - a_{ij}. \quad (18)$$

We study first the convergence of the estimation error (17), and then use it in the dynamics of the static feedback error control. The aim consists in finding the gain matrix L , so that the estimation error e_k satisfies the following \mathcal{H}_∞ criterion

$$\|e\|_{\ell_2} \leq \sqrt{\mu \|w\|_{\ell_2}^2 + \nu \|e_0\|^2}. \quad (19)$$

where $\mu > 0$ is the gain from w to e and $\nu > 0$ is to be determined.

Usually, a quadratic Lyapunov function is used to analyze the \mathcal{H}_∞ stability of the error

$$V_k(e_k) = e_k^T P e_k, \quad P = P^T > 0. \quad (20)$$

Consequently the \mathcal{H}_∞ criterion is satisfied if the following inequality holds

$$\mathcal{W}_k \triangleq \Delta V_k + \|e_k\|^2 - \mu \|w_k\|^2 \leq 0, \quad (21)$$

where $\Delta V_k = V(e_{k+1}) - V(e_k)$.

The following theorem gives the conditions that guarantee the asymptotic stability and the \mathcal{H}_∞ performance criterion of the estimation error in (17).

Theorem 2. If there exist symmetric positive definite matrices $P \in \mathbb{R}^{n \times n}$, $\mathbb{S}_{ij} \in \mathbb{R}^{n_i \times n_i}$, $i = 1, \dots, n$ and matrix $\mathcal{X} \in \mathbb{R}^{n \times n}$ of appropriate dimensions, so that the following LMI condition holds

$$\min(\mu) \text{ subject to (23)} \quad (22)$$

$$\begin{bmatrix} \mathbb{M} & \begin{bmatrix} \Pi_1^T & \dots & \Pi_p^T \end{bmatrix} \\ \begin{bmatrix} \star & & \end{bmatrix} & -\Lambda \mathbb{N} \end{bmatrix} < 0, \quad (23)$$

where

$$\mathbb{M} = \begin{bmatrix} -P + \mathbb{I} & 0 & A^T P - C^T \mathcal{X} \\ \star & -\mu \mathbb{I} & E^T P - D^T \mathcal{X} \\ \star & \star & -P \end{bmatrix}, \quad (24)$$

$$\begin{aligned} \Pi_i &= \left[\Pi_{i1}^T(\mathcal{X}, \mathbb{S}_{i1}) \dots \Pi_{in_i}^T(\mathcal{X}, \mathbb{S}_{in_i}) \right]^T, \\ \Pi_{ij}^T(\mathcal{X}, \mathbb{S}_{ij}) &= \begin{bmatrix} 0 \\ 0 \\ \mathcal{X}^T \mathcal{H}_{ij} \end{bmatrix} + \begin{bmatrix} H_i^T \\ 0 \\ 0 \end{bmatrix} \mathbb{S}_{ij} \end{aligned} \quad (25)$$

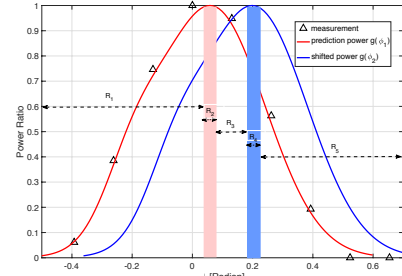


Fig. 7. Regions around slope-change points of $g(\phi)$ with $\Delta\phi = 8^\circ$.

$$\Lambda = \text{block-diag}(\Lambda_1, \dots, \Lambda_p), \quad (26)$$

$$\Lambda_i = \text{block-diag} \left(\frac{2}{\tilde{b}_{i1}} \mathbb{I}_{n_i}, \dots, \frac{2}{\tilde{b}_{in_i}} \mathbb{I}_{n_i} \right), \quad (27)$$

$$\mathbb{N} = \text{block-diag}(\mathbb{N}_1, \dots, \mathbb{N}_p), \quad (28)$$

$$\mathbb{N}_i = \text{block-diag}(\mathbb{N}_{i1}, \dots, \mathbb{N}_{in_i}), \quad (29)$$

then, the estimation error system in (17) is asymptotically stable and the \mathcal{H}_∞ performance criterion (19) is guaranteed with $\nu = \lambda_{\max}(P)$. In addition, the observer gain L is computed as

$$L = P^{-1} \mathcal{X}^T. \quad (30)$$

Proof. The proof is omitted due to space constraints.

4. SWITCHED-GAIN NONLINEAR OBSERVER FOR NON-MONOTONIC SYSTEMS

Recently, it has been proven in (Movahedi et al. (2019); Rajamani et al. (2020)) that in this situation with non-monotonic nonlinear functions, a single observer gain that guarantees exponentially stable estimation over the entire operating range cannot be found. Hence, the angular position range is divided piecewise into different regions. In each region, at least one of the angular output functions is a monotonic function of position. Fig. 7 illustrates a piecewise division of the angular position range into regions R_1 to R_5 due to the monotonicity concept.

We note that the boundaries of the regions lie at the slope change points (of one or the other received angular output function). For example, R_2 is a narrow region in which the slope of the output $g(\phi_1)$ is close to zero. In this region, only the output $g(\phi_2)$ will be used by the observer, since $g(\phi_2)$ is monotonic in this region. Regions R_1 and R_3 lie on either side of R_2 and both of these regions can utilize both outputs $g(\phi_1)$ and $g(\phi_2)$. Both $g(\phi_1)$ and $g(\phi_2)$ are monotonic in these regions.

Since each region, R_1 through R_5 has monotonic angular output function properties, as illustrated in Fig. 7. Then, a constant stabilizing observer gain exists in each of these regions. Now, consider a hybrid observer with a constant-gain L_1 in the region 1 designed using the LMI of equation (23) and the corresponding value of the Lyapunov positive definite matrix is P_1 as shown in Fig. 8. Likewise, L_2 is the observer gain in the region 2 and has the positive definite Lyapunov function matrix P_2 , as illustrated in Fig. 8. Here, y_{switch} is the nominal switching point between the two regions, and the variable ε is the hysteresis added to the switching to ensure a minimum dwell time after each

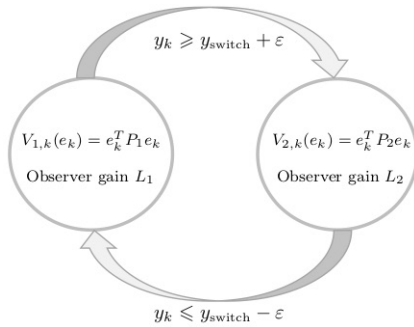


Fig. 8. Hybrid observer with switched gains around slope-change points of $g(\phi)$.

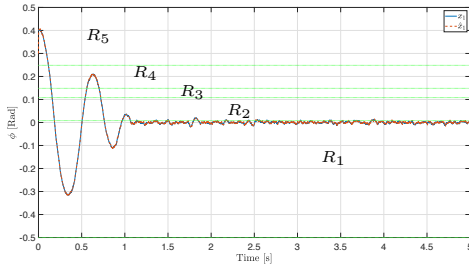


Fig. 9. Estimated angular position along with the actual angular position.

switch (Movahedi et al. (2019); Rajamani et al. (2020)). The stability of the hybrid observer of Fig. 8 consisting of different constant observer gain regions needs to be considered. Let the two observers be designed to be asymptotically stable in each of the two regions using the Lyapunov function analysis of Theorem 2. Then, it should be noted that inside each region, a single observer gain is used, and asymptotic stability is guaranteed. Furthermore, the stability of the overall switched system can be guaranteed if the system satisfies a minimum dwell time constraint in each region, according to results from hybrid system theory.

5. NUMERICAL SIMULATIONS

The effectiveness of the proposed nonlinear hybrid observer-based tracking is applied to the LED-based optical communication system. The discrete-time hybrid observer for estimating the angular position and velocity of the receiver orientation is designed as (13) and based on Theorem 2. The switched-gain nonlinear observer-based tracking along with the real angular position of the system is shown in Fig. 9. As seen in Fig. 9, the switched nonlinear observer exhibits good performance. Fig. 10 shows the estimated velocity position along with the actual velocity position using the proposed non-monotonic nonlinear observer method. Furthermore, the estimated angular position and velocity closely follow the actual zero reference value, as shown in Figs. 9 and 10, respectively. Besides, the proposed robust nonlinear hybrid observer is robust and can handle process disturbances and measurement noises for the LED-based optical communication application.

6. CONCLUSION

This paper focused on a robust observer-based tracking control design for a LED-based optical communication system with non-monotonic nonlinear measurement equations. Sufficient conditions for the asymptotic stability and

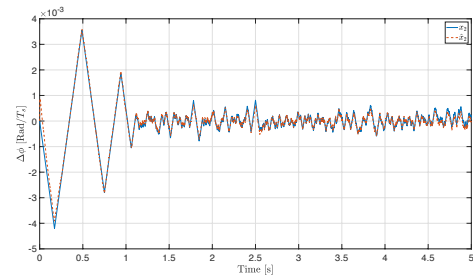


Fig. 10. Estimated velocity position along with the actual velocity position.

the \mathcal{H}_∞ performance criterion of the estimation error dynamics proposed are guaranteed using Lyapunov-analysis. Based on the state estimate, a static feedback controller is updating to drive the mean of the receiver orientation to zero. Due to space constraints, the proofs of the technical results are omitted.

REFERENCES

- Doniec, N., Angermann, M., and Rus, D. (2013). An end-to-end signal strength model for underwater optical communications. *IEEE Journal of Ocean. Eng.*, 38(4), 743–757.
- Draa, K.C., Zemouche, A., Alma, M., Voos, H., and Darouach, M. (2019). A discrete-time nonlinear state observer for the anaerobic digestion process. *International Journal of Robust and Nonlinear Control*, 29(5), 1279–1301.
- Ghassemlooy, Z., Popoola, W., and Rajbhandari, S. (2012). *Optical Wireless Communications: System and Channel Modelling with MATLAB*. CRC Press, Berlin, 1st edition.
- Hagem, R., Thiel, D.V., O’Keefe, S., Wixted, A., and Fickenscher, T. (2011). Low cost short-range wireless optical FSK modem for swimmers feedback. In *IEEE Sensors Conf.* Los Angeles, CA, USA.
- Hanson, F. and Radic, S. (2008). High bandwidth underwater optical communication. *Appl. Opt.*, 47(2), 277–283.
- Ivan, M. and Ching-Cherng, S. (2008). Modeling the radiation pattern of LEDs. *Optics Express*, 16(3), 1808.
- Lu, F., Lee, S., Mounzer, J., and Schurgers, C. (2009). Low-cost medium-range optical under water modem. In *4th ACM Int. Workshop Under Water Network*, 1–11. Los Angeles, CA, USA.
- Miller, F., Vandome, A., and McBrewster, J. (2009). *Beer-Lambert Law*. VDM Publishing, Saarbrücken, Germany.
- Movahedi, H., Zemouche, A., and Rajamani, R. (2019). Linear position estimation on smart actuators using a nonlinear observer. In *American Control Conference*. Philadelphia, USA.
- Rajamani, R., Jeona, W., Movahedi, H., and Zemouche, A. (2020). On the need for switched-gain observers for non-monotonic nonlinear systems. *Automatica*, 114, 108814.
- Solanki, P.B., Al-Rubaiaai, M., and Tan, X. (2016). Extended Kalman filter-aided alignment control for maintaining line of sight in optical communication. In *Proc. Amer. Control Conf.*, 4520–4525.
- Solanki, P.B., Al-Rubaiaai, M., and Tan, X. (2018). Extended Kalman filter-based active alignment control for LED optical communication. *IEEE/ASME Transactions on Mechatronics*, 23(4), 1501–1511.